iScience

CellPress
OPEN ACCESS

Article

Estrogen receptor alpha regulates uterine epithelial lineage specification and homeostasis

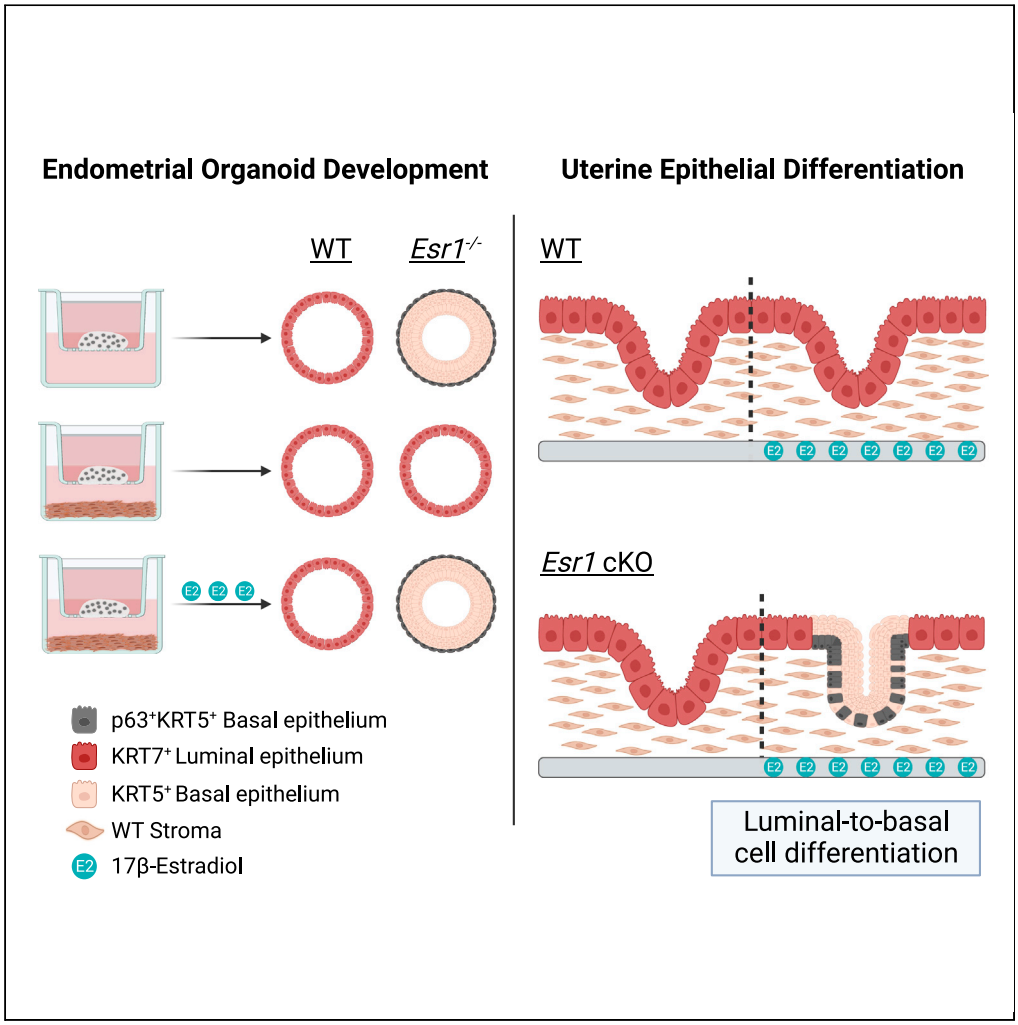

Jason A. Rizo, Kimberly M. Davenport, Wipawee Winuthayanon, Thomas E. Spencer, Andrew M. Kelleher

andrew.kelleher@missouri.edu

Highlights

ESR1 is required for uterine epithelial organoid development

Absence of epithelial ESR1 drives luminal-to-basal differentiation

Endometrial stromal cells govern ESR1-negative epithelial plasticity

Stroma-mediated E2 signaling impacts ESR1-negative epithelial differentiation

Rizo et al., iScience 26, 107568
September 15, 2023
https://doi.org/10.1016/j.isci.2023.107568

iScience

CellPress
OPEN ACCESS

Article

Estrogen receptor alpha regulates uterine epithelial lineage specification and homeostasis

Jason A. Rizo,[1] Kimberly M. Davenport,[1] Wipawee Winuthayanon,[2] Thomas E. Spencer,[1,2] and Andrew M. Kelleher[2,3,*]

SUMMARY

Postnatal development of the uterus involves specification of undifferentiated epithelium into uterine-type epithelium. That specification is regulated by stromal-epithelial interactions as well as intrinsic cell-specific transcription factors and gene regulatory networks. This study utilized mouse genetic models of *Esr1* deletion, endometrial epithelial organoids (EEO), and organoid-stromal co-cultures to decipher the role of *Esr1* in uterine epithelial development. Organoids derived from wild-type (WT) mice developed a normal single layer of columnar epithelium. In contrast, EEO from *Esr1* null mice developed a multilayered stratified squamous type of epithelium with basal cells. Co-culturing *Esr1* null epithelium with WT uterine stromal fibroblasts inhibited basal cell development. Of note, estrogen treatment of EEO-stromal co-cultures and *Esr1* conditional knockout mice increased basal epithelial cell markers. Collectively, these findings suggest that *Esr1* regulates uterine epithelium lineage plasticity and homeostasis and loss of ESR1 promotes altered luminal-to-basal differentiation driven by ESR1-mediated paracrine factors from the stroma.

INTRODUCTION

The female reproductive tract develops from the Müllerian duct and contains different types of epithelia in the oviduct, uterus, cervix, and vagina.[1] In mice, development of the uterus is only completed after birth.[1,2] During the first week, the multipotent epithelium of the uterus becomes specified into a simple columnar type of luminal epithelium (LE), and the mesenchyme stratifies into stroma and myometrium. During the second week, the glandular epithelial (GE) cells arise from LE stem progenitor cells and tubular gland morphogenesis is initiated.[3] Tissue recombination studies established the importance of mesenchyme/stroma to instruct epithelial differentiation in the female reproductive tract.[4,5] Specifically, paracrine factors from mesenchymal cells in the caudal region of the Müllerian duct trigger expression of the transcription factor p63 (*Trp63*) in the epithelium,[6–8] leading to the differentiation of the cervix and vagina with a multilayered stratified type of epithelium containing basal cells.[9] Of note, the simple columnar-type luminal epithelium of the uterus does not express *Trp63*. *Trp63* null mice lack basal cells in the cervicovaginal epithelium, supporting the idea that p63 is a master regulator of epithelial cell lineage specification in the Müllerian duct.[10]

The role of estrogen receptor alpha (*Esr1*) in postnatal epithelial differentiation and homeostasis in the uterus is not fully understood. *Esr1* is expressed in all cells of the myometrium, stroma, and epithelium of the adult uterus.[11,12] Although *Esr1* is dispensable for embryonic Müllerian duct patterning and differentiation into the uterus,[12,13] it is essential for postnatal uterine gland maintenance and control of epithelial apoptosis in the adult uterus.[11,14,15] Interestingly, *Esr1* is not expressed in the developing epithelium of the uterus during the first week after birth.[16] However, neonatal exposure to the diethylstilbestrol, a potent ESR1 agonist, altered differentiation of the uterus and induced squamous metaplasia in a p63-dependent manner.[10] Intriguingly, *Trp63* expression is augmented and expanded in cervicovaginal epithelium in the absence of *Esr1*.[17] While these data support the idea that *Esr1* may regulate postnatal uterine epithelial development, further interrogation of the impact of *Esr1* is required to explain the previous findings.

Organoid culture is a valuable model system for investigating the cell autonomous regulation of epithelial differentiation and physiology.[18,19] Organoids derived from different areas of the mouse reproductive tract have been established, including the oviduct,[20,21] uterus,[22,23] cervix,[24,25] and vagina.[26,27] These organoids maintain phenotypic and morphological features of their organs of origin.[20,23,24,27] Characterization and analysis of organoid formation in these models enable the identification of biomarkers and mutations associated with organ development and function,[23,28] which can be leveraged to uncover the mechanisms underlying normal and abnormal epithelial development in the female reproductive tract.

[1]Division of Animal Sciences, University of Missouri, Columbia, MO 65211, USA
[2]Department of Obstetrics, Gynecology, and Women's Health, University of Missouri, Columbia, MO 65211, USA
[3]Lead contact
*Correspondence: andrew.kelleher@missouri.edu
https://doi.org/10.1016/j.isci.2023.107568

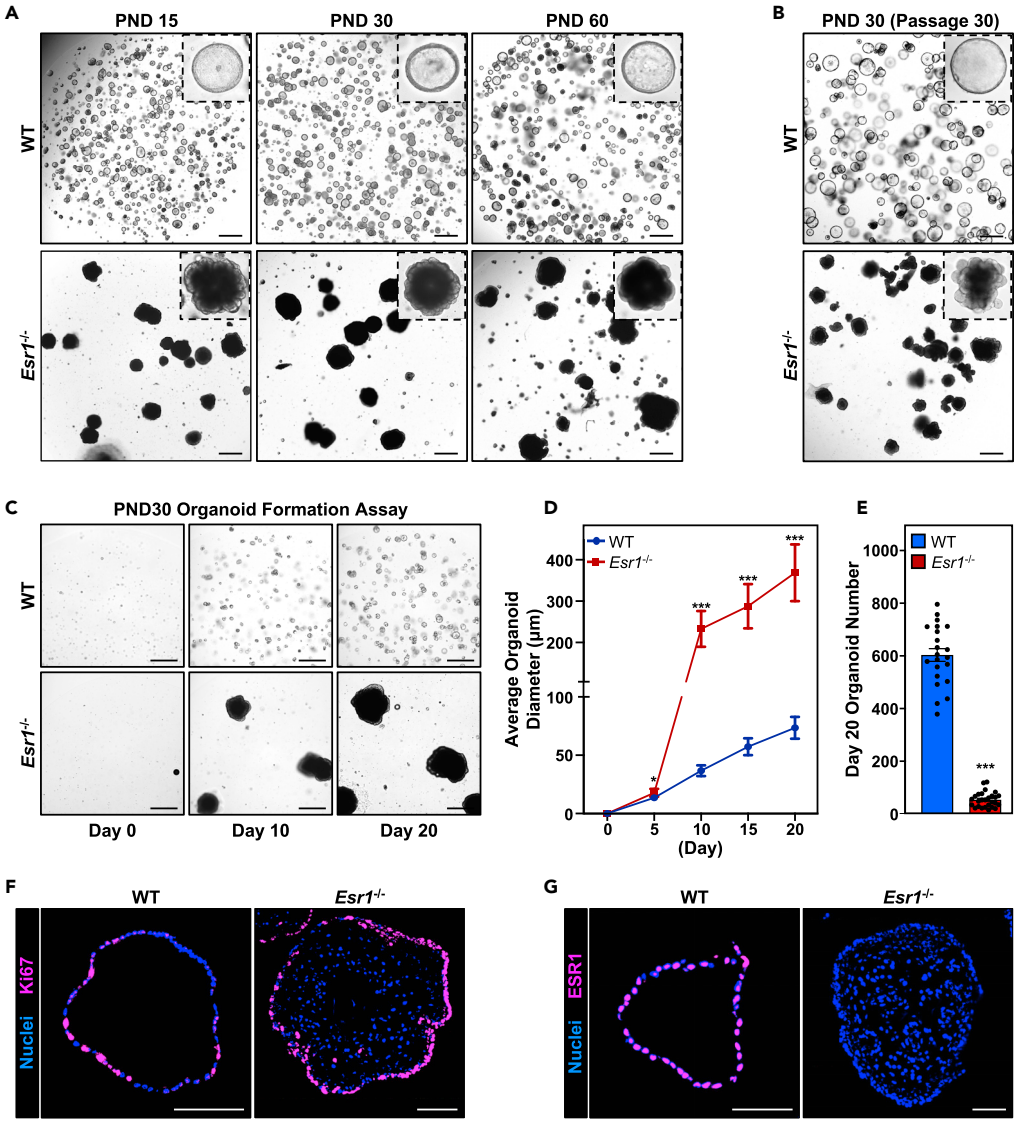

Figure 1. Derivation and characterization of *Esr1*$^{-/-}$ endometrial epithelial organoids

(A) Brightfield images of organoids established from WT and *Esr1*$^{-/-}$ females at postnatal days (PND) 15, 30, and 60. (Scale bars, 500 μm).

(B) Brightfield images demonstrating long-term expansion potential and gross morphology of WT and *Esr1*$^{-/-}$ organoids at passage 30. (Scale bars, 500 μm).

(C) Representative images from the organoid formation assay from single cells expanded for 20 days (scale bars, 500 μm).

(D and E) Quantification of average organoid diameter (D) and total organoid number (E).

(F and G) Immunofluorescent localization of Ki67 (F) and ESR1 (G) (Scale bars, 100 μm). All experiments were performed on passage 3 organoids (n ≥ 3 mice per genotype). Data are presented as mean ± S.E.M. Solid dots represent individual drops in technical replicates. *p < 0.05 and ***p < 0.001 (Student's *t* test).

Here, a comprehensive set of studies involving endometrial epithelial organoids (EEO), co-culture of uterine stromal and epithelial cells, and mouse genetic models of *Esr1* deletion were employed to understand the biological role of ESR1 in uterine epithelium development. The findings reveal that loss of *Esr1* in the epithelium of the uterus results in the activation of a basal differentiation program that is mediated by E2-dependent paracrine factors from the stroma.

RESULTS

Impact of ESR1 on epithelial differentiation in mouse organoids

EEO were established from global *Esr1* null (*Esr1*$^{-/-}$) mice[12] and wild-type (WT) littermate control mice on postnatal days (PND) 15, 30, and 60 (Figure 1A). Epithelial cells were isolated through enzymatic digestion and cultured in a basement membrane extract (BME) under WNT-activating conditions using described STAR Methods.[22] Efficient establishment of EEO was observed from both genotypes at all

ages under these conditions; however, distinct differences in morphology were noted between genotypes (Figure 1A). EEO derived from the uteri of WT mice were spherical with a discernible lumen, whereas those generated from *Esr1*$^{-/-}$ mice were larger, denser, and lobular (Figure 1A). ESR1 was abundant in WT EEO but absent in EEO developed from *Esr1*$^{-/-}$ epithelium (Figure S1). The EEO derived from PND 30 uteri of both genotypes could be expanded for 30 passages over a 6-month period (Figure 1B). Thus, ESR1 absence does not affect long-term organoid expansion and phenotype based on morphology.

Passage 2 WT and *Esr1*$^{-/-}$ EEO from PND 30 uteri were dissociated into single cells (Figure S2) and 5,000 cells were placed into equal amounts of BME. After 20 days of culture, 12.1% of WT cells, but only 1.2% of *Esr1*$^{-/-}$ cells, formed EEO (Figures 1C–1E). Although fewer EEO formed from *Esr1*$^{-/-}$ uterine epithelial cells (Figure 1E), the organoids were larger in diameter (Figures 1C and 1D) and contained greater numbers of Ki67-positive proliferative cells (41.9% vs. 26.2%) (Figure 1F). Histologically, the WT EEO contained a single layer of columnar-type epithelial cells, whereas the cells of *Esr1*$^{-/-}$ EEO were multilayered (Figures 1F and 1G).

Alterations in the transcriptome of *Esr1* null organoids

The transcriptome was assessed by RNA-seq using passage 3 EEO established from the uterine epithelium of PND 30 WT and *Esr1*$^{-/-}$ mice. As illustrated in Figure 2A, 2,729 transcripts were classified as differentially expressed genes (DEGs) using specific criteria (Log2 fold change >2, FDR <0.05, and mean CPM >1) (Table S1). mRNA transcripts of genes were increased (2,016) and decreased (713) in *Esr1*$^{-/-}$ as compared to WT EEO (Figure S3A). Gene set enrichment analysis of the increased genes revealed biological processes associated with keratinization, keratinocyte differentiation, epidermal cell differentiation, and epithelium development (Figure 2A). In contrast, genes with decreased mRNA transcript abundance were enriched for pathways involved in glycoprotein and carbohydrate metabolic processes, protein glycosylation, regulation of cell migration, transmembrane transport, and tissue development. Network analysis determined the relationship between the top biological processes enriched in *Esr1*$^{-/-}$ EEO and identified genes belonging to the epidermal differentiation complex (EDC) (Figure S3B). The EDC family of genes is required for the terminal differentiation of basal epithelial cells and includes *S100* genes, small proline-rich (*Sprr*) genes, late cornified envelope (*Lce*) genes, and filaggrin-like genes (*Flg*, *Rptn*, and *Tchh*).[29–31] The mRNA transcripts corresponding to those EDC genes were much more abundant in *Esr1*$^{-/-}$ than WT EEO (Figures S3C–S3F). Additionally, many of the DEGs with increased mRNA levels regulate keratinocyte differentiation and encode main structural components of the cornified envelope in squamous epithelium (*Bcl11b*, *Ivl*, *Lor*)[32–34] (Figure S3G).

Upstream transcription factor binding analysis of DEGs was performed using ChEA3.[35] The top transcription factor was predicted as ESR1 for the genes with higher expression in WT EEO. Interestingly, the same analysis performed on DEGs that increased in *Esr1*$^{-/-}$ EEO uncovered significant enrichment for p63 (Figure S3H). p63 is an identity switch for Müllerian duct epithelium to be cervicovaginal versus uterine[9] and directly regulates the expression of basal keratin genes.[36,37] Indeed, expression of many basal keratins (*Krt1*, *Krt5*, *Krt6*, *Krt10*, *Krt13*, *Krt14*, *Krt15*, *Krt16*, *Krt17*, *Krt75*, and *Krt78)* was much more abundant in *Esr1*$^{-/-}$ EEO (Figure 2B), whereas expression of luminal keratins (*Krt7* and *Krt18)*[38] was much lower or absent in *Esr1*$^{-/-}$ EEO (Figure 2B).

As illustrated in Figure 2C, *Esr1*$^{-/-}$ EEO possessed high levels of basal KRT5 and p63 proteins, but not luminal KRT7, in their multilayered cells. In contrast, WT EEO contained a single layered epithelium that expressed luminal KRT7 with no evidence of p63 (Figure 2C). The *Esr1*$^{-/-}$ organoid phenotype resembles the multilayered organoids developed from cervicovaginal tissues, as both were multilayered with similar patterns of p63, Ki67, and KRT5 expression[24,27] (Figures 1A–1F and 2C). FOXA2, a transcription factor specific to GE cells of the mouse and human uterus,[3] is also present in all cells of the cervical epithelium.[39] Nuclear FOXA2 was present in all cells of the *Esr1*$^{-/-}$ EEO (Figure 2C), but only in a few cells in the WT EEO. Western blot analysis of EEO confirmed the increase of FOXA2 in *Esr1*$^{-/-}$ EEO (Figure S1). Thus, the gene expression signature of the *Esr1*$^{-/-}$ EEO signifies cervicovaginal type of epithelium, which is a multilayered stratified squamous epithelium that contains a mitotically active basal layer and a superficial layer of cornified cells with basal-type keratins.[40]

Stromal cells impact *Esr1*$^{-/-}$ organoid differentiation

Stromal-derived paracrine factors impact epithelial proliferation, differentiation, and function in the female reproductive tract and other epitheliomesenchymal organs.[6–8] Elegant tissue recombination studies using cells from the uterus and vagina discovered that the mesenchyme/stroma instructs the undetermined multipotent female reproductive tract epithelium to differentiate into uterine (simple columnar) or cervicovaginal (stratified squamous with basal cells) epithelium.[4,5,10] Thus, an *in vitro* co-culture system was established to study effects of stromal-derived factors on epithelial cell growth and differentiation into organoids (Figure 3A). All experiments used WT stroma, as we were not able to obtain sufficient quantities of *Esr1*$^{-/-}$ stroma cells. Uterine epithelia from WT or *Esr1*$^{-/-}$ null mice were placed into BME on a transwell cell culture insert that was then placed in a well containing WT stroma cells or no stroma cells as a control (Figure 3A). Over a 20 days growth period, the WT epithelial cells formed EEO with normal growth and single layer morphology, and the presence of WT stromal cells had no discernible effects on the morphology of WT EEO (Figures 3B and 3C). As expected, *Esr1*$^{-/-}$ epithelial cells formed larger, denser, and lobular structures in the absence of stroma (Figures 3B and 3C) that expressed cervicovaginal-type epithelium markers (*Trp63*, *Krt5*, and *Krt14*) (Figure 3D). In contrast, *Esr1*$^{-/-}$ epithelial cells cultured with WT stroma formed EEO that exhibited morphology more similar to EEO from WT (*Esr1*$^{+/+}$) uterine epithelium (Figure 3B) and lacked expression of cervicovaginal-type epithelium markers (*Trp63*, *Krt5*, and *Krt14*) (Figure 3D). Thus, the ESR1-expressing WT stroma produces paracrine factors that impact growth and differentiation of *Esr1*$^{-/-}$ epithelia.

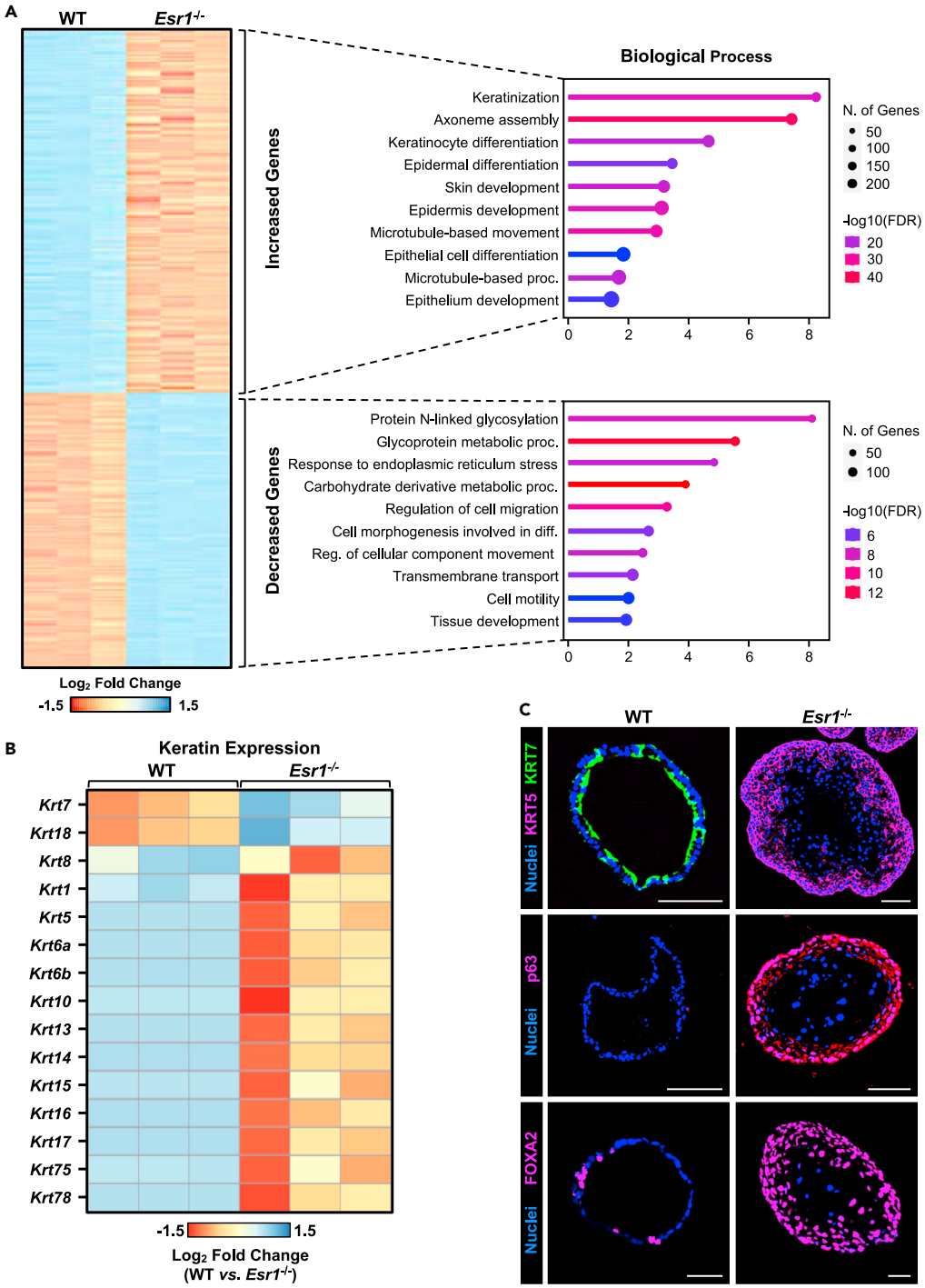

Figure 2. Absence of *Esr1* alters EEO gene expression

RNA was isolated from passage 3 organoids established from individual PND 30 mice.

(A) Heatmap of DEGs and visualization of biological process GO terms associated with genes differentially expressed in $Esr1^{-/-}$ and WT organoids based on RNA-seq analysis.

(B) Heatmap of differential keratin expression in $Esr1^{-/-}$ organoids.

(C) Immunofluorescent localization for basal (KRT5/p63) or luminal (KRT7) cell markers, and for the uterine gland-specific marker FOXA2. (Scale bars, 100 μm).

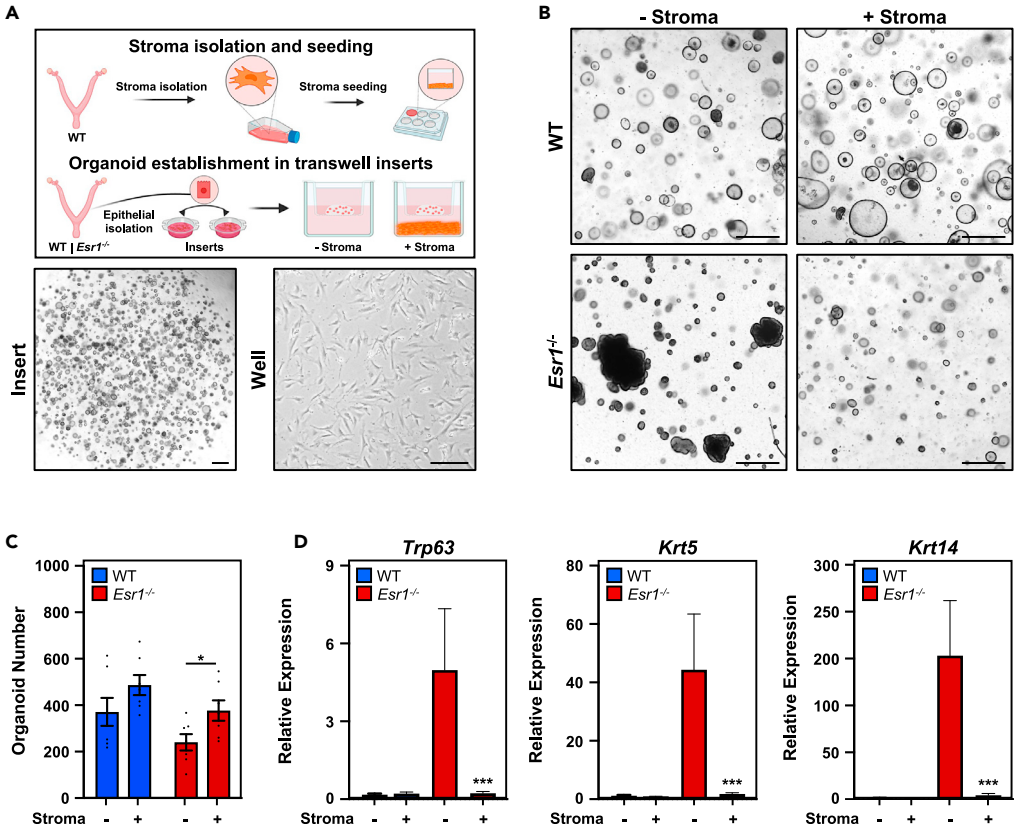

Figure 3. Stromal-epithelial co-culture impacts *Esr1*$^{-/-}$ organoid development

(A) Experimental design. Epithelial cells were seeded in Cultrex on transwell inserts over a bed of stromal fibroblasts adhered to the bottom of 6 well plates and cultured for 20 days (n ≥ 5 mice per genotype).

(B) Representative brightfield images at day 20 of culture (scale bars, 500 μm).

(C) Quantification of the number of organoids at day 20 of culture. Solid dots represent average organoid number per biological replicate.

(D) RT-qPCR analysis for the basal cell markers *Trp63*, *Krt5*, and *Krt14* (n = 3 mice per genotype/treatment). Data are presented as fold change compared to WT EEO cultured in the absence of stromal fibroblasts. *p < 0.05 and ***p < 0.001 (Student's *t* test).

ESR1 loss *in vivo* alters differentiation of the uterine epithelium

Based on our *in vitro* 3D organoid observations, studies of uterine epithelium were performed in WT, *Esr1*$^{-/-}$, and *Esr1* conditional knockout (cKO) mice (Figure 4A). In the *Pgr*^{Cre} model,[41] the Cre is active by PND 3 in the uterus and deletes floxed genes in both uterine epithelium and stroma (Figure 4A). On PND 60, no basal keratins (KRT5 and KRT14) or p63-expressing cells were observed in the uteri of either WT, *Esr1*$^{-/-}$, or *Pgr*$^{Cre/+}$*Esr1*$^{f/f}$ females (Figures 4B–4D). As expected, endometrial organoids established from *Pgr*$^{Cre/+}$*Esr1*$^{f/f}$ mice developed into large, dense, and lobular structures (Figure 4A), replicating the phenotype of *Esr1*$^{-/-}$ EEO.

The lack of epithelial proliferation in the *Esr1*$^{-/-}$ mouse uterus[11,12] may hinder epithelial differentiation toward the basal cell lineage. Moreover, several studies have indicated that epithelial cell proliferation and differentiation are regulated by paracrine signaling from the stroma.[4,13] To determine the impact of disrupted stromal-epithelial crosstalk on epithelial differentiation in the absence of epithelial *Esr1*, the epithelial-specific *Wnt7a*^{Cre}[14] and GE-specific *Foxa2*^{Cre}[42] mouse models were used to conditionally delete *Esr1* in endometrial epithelial cells. *Wnt7a*^{Cre} is active in the Müllerian duct epithelium of the embryo, whereas *Foxa2*^{Cre} should be active only in the differentiating and developing GE.[43–47] Indeed, *Wnt7a*$^{Cre/+}$*Esr1*$^{f/f}$ deletes *Esr1* in only the uterine LE and GE cells but not the stroma or myometrium.[14] As expected, ESR1 was undetectable in the glands of adult *Foxa2*$^{Cre/+}$*Esr1*$^{f/f}$ mice but was observed in the pseudostratified LE and stroma (Figure 4A). *Foxa2*$^{Cre/+}$*Esr1*$^{f/f}$ females failed to achieve pregnancies and displayed complete infertility in a 6-month breeding trial (Table S2). On PND 60, the uterus of *Foxa2*$^{Cre/+}$*Esr1*$^{f/f}$ mice contained areas of squamous metaplasia with a multilayered epithelium only in the glands, whereas the glands of the uterus from WT, *Esr1*$^{-/-}$, or *Pgr*$^{Cre/+}$*Esr1*$^{f/f}$ females were normal with a simple columnar-type epithelium (Figures 4A–4D). The glands of *Foxa2*$^{Cre/+}$*Esr1*$^{f/f}$ uteri exhibiting squamous metaplasia contained KRT5, KRT14, and p63-positive basal cells (Figures 4B–4D). Further, EEO generated from epithelial cells isolated from uteri of *Foxa2*$^{Cre/+}$*Esr1*$^{f/f}$ mice displayed a mixture of phenotypes including larger, dense, multilayered, and lobular organoids typical of *Esr1*$^{-/-}$ EEO and smaller, spherical, and single-layered EEO typical of WT mice (Figure 4A).

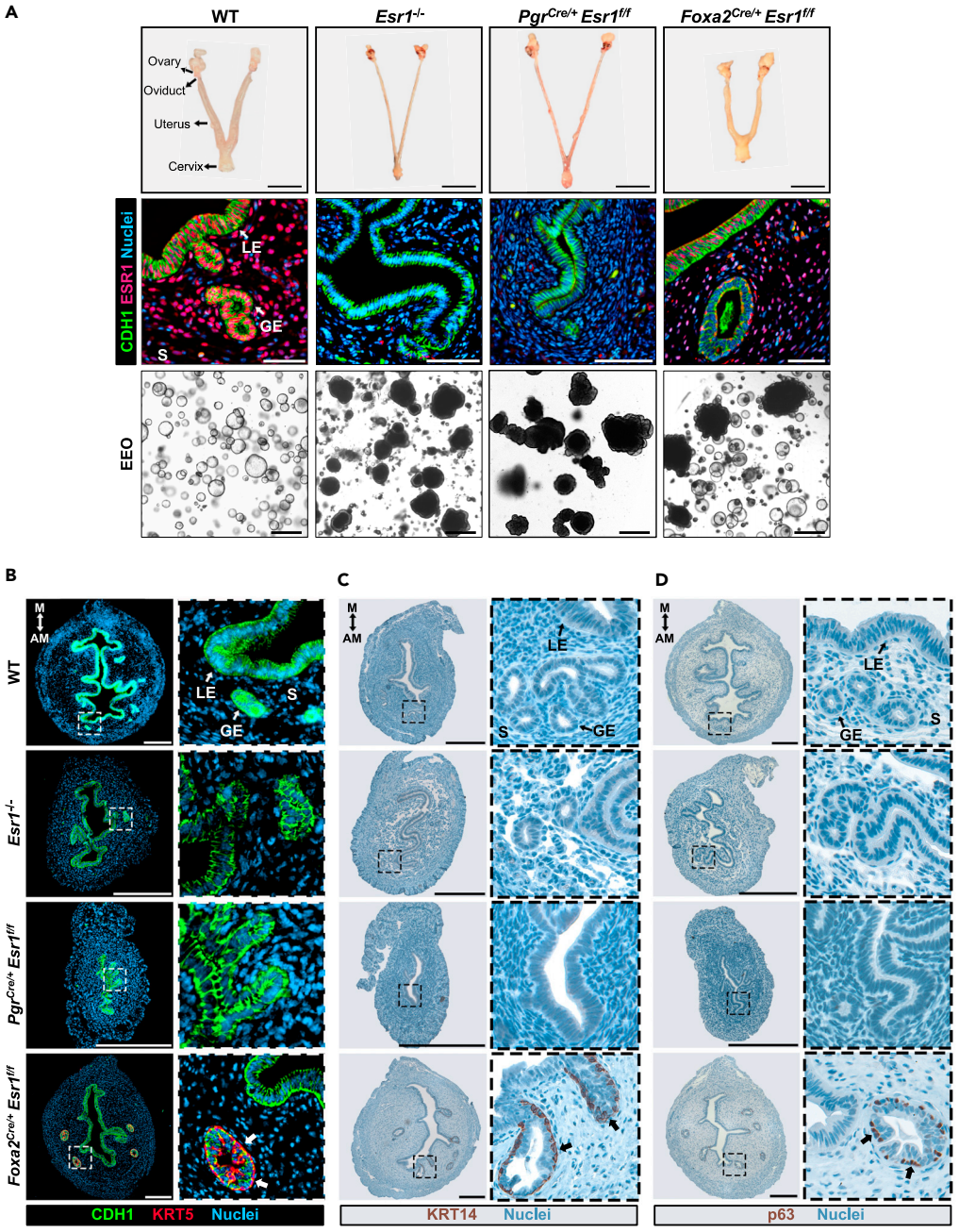

Figure 4. Epithelial *Esr1* deletion results in a stratified uterine epithelial layer

(A) Top panel: uteri of PND 60 $Esr1^{f/f}$ (WT), $Esr1^{-/-}$, $Pgr^{Cre/+}Esr1^{f/f}$, and $Foxa2^{Cre/+}Esr1^{f/f}$ mice (scale bars, 1 cm). Middle panel: ESR1 immunolocalization in uterine cross-sections (scale bars, 100 μm). Bottom panel: gross morphology of passage 3 endometrial epithelial organoids (EEO) (scale bars = 500 μm).

(B–D) Immunolocalization of the basal markers KRT5 (B), KRT14 (C), and p63 (D) (scale bars, 250 μm). For (B), (C), and (D), panels on the left show uterine cross-sections and dashed panels on the right are insets of luminal and glandular epithelium. White and black arrows indicate the presence of basal cells in the uterine glandular epithelium of $Foxa2^{Cre/+}Esr1^{f/f}$ mice (n ≥ 3 mice/genotype). LE, luminal epithelium; GE, glandular epithelium; S, stroma; M, mesometrial; AM, antimesometrial.

Adult $Wnt7a^{Cre/+}Esr1^{f/f}$ uteri also possessed KRT5-positive cells, but they were present in both the LE and glands (Figure S4A). Organoids generated from the uterine epithelial cells of $Wnt7a^{Cre/+}Esr1^{f/f}$ mice displayed the same morphology as $Pgr^{Cre/+}Esr1^{f/f}$ and $Esr1^{-/-}$ EEO and were dense, multilayered, and lobular (Figure S4C). Areas of the LE and all GE of uteri from $Wnt7a^{Cre/+}Esr1^{f/f}$ mice were positive for FOXA2, which is atypical as FOXA2 is not present in the uterine LE of WT mice[46] (Figure S4B). This is consistent with previous observations in $Wnt7a^{Cre/+}Esr1^{f/f}$ mice where FOXA2 is upregulated in the ESR1-negative uterine luminal and vaginal epithelium.[48] In WT mice, FOXA2 is

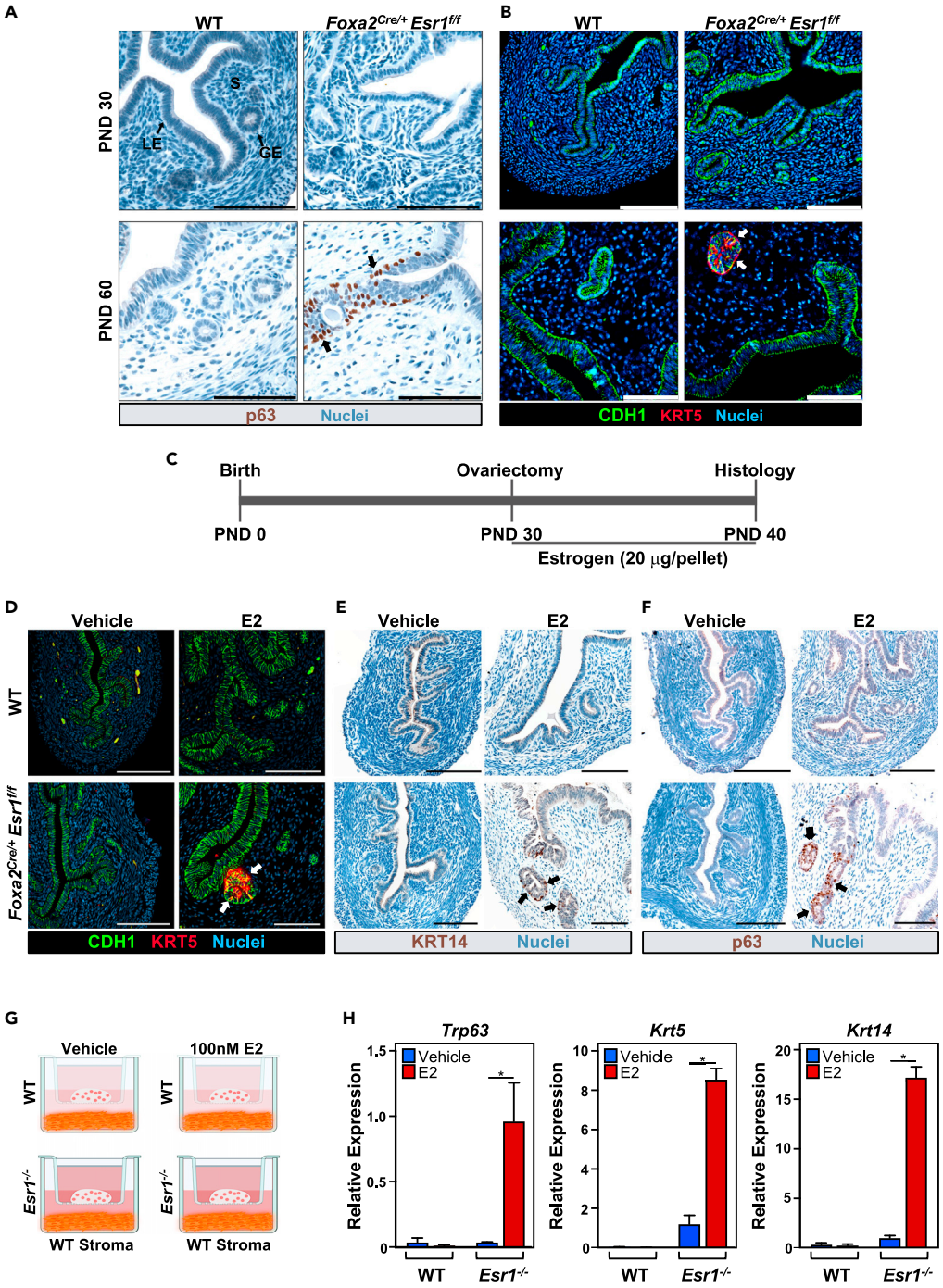

Figure 5. Basal cell differentiation in the uterine epithelium is mediated by E2 actions on the stroma

(A and B) Immunolocalization of p63 (A) and KRT5 (B) in uterine cross-sections of *Esr1*$^{f/f}$ (WT) and *Foxa2*$^{Cre/+}$*Esr1*$^{f/f}$ mice. Histological analysis was performed on PND 30 (top panels) and PND 60 (bottom panels) females (scale bars, 100 μm). White and black arrows indicate the presence of basal cells in the uterine glandular epithelium. LE, luminal epithelium; GE, glandular epithelium; S, stroma.

(C) Experimental design. *Esr1*$^{f/f}$ (WT) and *Foxa2*$^{Cre/+}$*Esr1*$^{f/f}$ females were ovariectomized (OVX) at PND 30 and supplemented with E2 (20 μg/pellet) for 10 days.

(D–F) Immunolocalization of the basal markers KRT5 (D), KRT14 (E), and p63 (F). White and black arrows indicate the presence of basal cells in the uterine glandular epithelium (scale bars, 100 μm).

Figure 5. *Continued*

(G) Experimental design for the co-culture experiment. Stromal cells isolated WT females were co-cultured with organoids established from individual WT or *Esr1*$^{-/-}$ mice (n = 3 females per genotype). Co-cultures were treated with vehicle (100% Ethanol) or 100 nM E2 for 20 days.

(H) RT-qPCR for the basal cell markers *Trp63*, *Krt5*, and *Krt14*. Gene expression data were normalized to *Actb* and *Ppia* mRNA and are presented as mean relative expression in comparison to the value of an appropriate control sample using the $2^{-\Delta Ct}$ method ±S.E.M. *, $p < 0.05$ (Student's *t* test) ($n \geq 3$ mice per genotype).

expressed in the upper layers of the stratified squamous-type epithelium of the cervix[39] and vagina.[48] Collective *in vivo* and *in vitro* results support the idea that *Esr1* expression in the uterine epithelium has a role in LE lineage specification, homeostasis, and developmental plasticity.

Estrogen effects on ESR1-negative uterine epithelial cell differentiation

Normal epithelial differentiation and gland development is observed in *Esr1*$^{-/-}$ mice from birth to PND 30; however, those mice lose glands and have reduced uterine cell proliferation between PNDs 30 and 60 in contrast to continued adenogenesis and proliferation observed in WT uteri.[11,12] Indeed, KRT5 and p63-expressing basal cells are not observed in PND 30 *Foxa2*$^{Cre/+}$*Esr1*$^{f/f}$ (*Foxa2* cKO) mice, but are observed at PND 60 (Figures 4B–4D, 5A, and 5B). In mice, ligand-dependent ESR1 signaling is crucial for uterine epithelial proliferation and function after puberty.[11,14,15] These collective results support the idea that E2 acts via the stroma to alter differentiation of the *Esr1*$^{-/-}$ epithelium in the uterus. To address that hypothesis, WT and *Foxa2*$^{Cre/+}$*Esr1*$^{f/f}$ females were ovariectomized (OVX) on PND 30 and treated for 10 days with either a sham implant as a control or E2 (Figure 5C). No evidence of epithelial stratification, basal keratins (KRT5, KRT14), or p63-positive cells was observed in the uteri of control or E2-treated WT mice (Figures 5D and 5F). In contrast, uteri from E2-treated *Foxa2*$^{Cre/+}$*Esr1*$^{f/f}$ mice displayed KRT5, KRT14, and p63-positive stratified cells in the glands. Thus, E2 causes abnormal epithelial differentiation in ESR1-negative epithelial cells of the uterus via paracrine factors emanating from the ESR1-positive stroma.

In vitro co-culture studies were then conducted to determine E2 effects on ESR1-negative uterine epithelial cell differentiation (Figure 5G). Epithelial cells were isolated from either WT or *Esr1*$^{-/-}$ uteri and placed in BME on cell culture inserts placed into wells containing stromal cells from WT uteri (Figure 5G). Organoid-stroma co-cultures were treated with 100 nM E2 or vehicle as a control for 20 days. Similar to results presented in Figure 3, both WT and *Esr1*$^{-/-}$ epithelial cells co-cultured with WT stroma formed EEO with single-layered cell morphology (Figures S5A and S5B). Treatment of co-cultures with E2 increased expression of basal cell markers (*Trp63*, *Krt5*, and *Krt14*) in *Esr1*$^{-/-}$ EEO but not WT EEO (Figure 5H). These results support the idea that E2 promotes basal cell differentiation and stratification of ESR1-negative uterine epithelial cells via paracrine factors produced by WT stromal cells.

DISCUSSION

These studies provide novel insights into the developmental plasticity of epithelia in the developing postnatal uterus and essential role of *Esr1* in regulating epithelial cell differentiation, maintaining luminal epithelial cell identity, and restricting cellular plasticity of specified uterine LE and GE cells. These findings also reinforce the importance of paracrine factors from the stroma in directing development, differentiation, and homeostasis of the epithelium in the uterus. These findings have important implications for how estrogens, ESR1 agonists, and ESR1 antagonists impact uterine function and the etiology of common endometrial-based diseases including infertility, uterine squamous metaplasia, adenomyosis, adenocarcinoma, and endometriosis.

Previous studies found that knockouts of *Esr1*, both global and cell type specific, impact postnatal uterine morphogenesis and growth as well as adult function through cell-specific actions. Uterine epithelial-specific conditional knockout mice defined differential cell type-specific roles for ESR1 and its contribution to epithelial function.[14,15] While *Esr1* is not necessary for uterine development, growth, and adenogenesis during the first month of life, maintenance of glands and cell proliferation is compromised in the uterus of global *Esr1*$^{-/-}$ mice during the second month after puberty.[11,12] The findings of the presented studies strongly support the idea that *Esr1* has a critical and unexplored role in uterine epithelial homeostasis and plasticity based on *in vivo* studies of the uterus and *in vitro* studies of organoids.

Organoids are biomimetic 3D mini-organs that can be developed from single cells or groups of cells *in vitro* using culture conditions involving BME and growth factors. Endometrial epithelial-based organoids are long-term expandable and retain properties of the original tissue while remaining genomically stable, which makes them useful tools to study mechanisms underlying epithelial development and function.[49] Mouse and human EEO established in BME and cultured under WNT-activating conditions form spheroids with a single layer of columnar-type epithelium and a central lumen. Human EEO contain both major LE and GE cell types as well as proliferative, stem, and secretory cell subtypes that are typical of endometrial epithelium of the cycling uterus.[22,50] In the present studies, epithelial cells from WT mice also formed spheroids with a single layer of epithelial cells that closely resembles *in vivo* epithelium of the uterus with both GE (FOXA2 positive, ESR1 positive) and LE cells (FOXA2 negative, ESR1 positive) as well as proliferating cell subtypes. In contrast, EEO established from uterine epithelial cells of *Esr1*$^{-/-}$ mice more closely resembled those of the stratified squamous-type epithelium of the ectocervix or vagina[24] with basal cells (p63, KRT5, and Ki67), parabasal cells (p63, KRT5), and terminally differentiated basal cells (*Krt5, Flg, Lor,* and *Bc11b*). Indeed, organoids derived from the epithelia of the mouse cervix and vagina also form stratified multilayered structures with basal and proliferative cells.[24,27]

Transcriptome analysis of *Esr1*$^{-/-}$ EEO revealed a significant upregulation of genes associated with basal epithelium differentiation, particularly those involved in keratinization and epidermal development. Notably, the expression of several epidermal differentiation complex (EDC) gene families, including the small proline-rich (*Sprr*), late cornified envelope (*Lce*), S100 fused-type protein, and S100 genes, as well as the main structural components of the cornified envelope in squamous epithelium, *involucrin (Ivl)* and *loricrin (Lor)*, was markedly increased in *Esr1*$^{-/-}$ EEO.[29,30] These genes encode proteins that participate in the cornification of stratified squamous epithelium present in the cervix

and vagina[32,33] and present in cervical organoids.[24] Enrichment of binding sites for p63, a known identity switch for Müllerian duct epithelium to be cervicovaginal versus uterine, was present in DEGs of *Esr1*$^{-/-}$ EEO.[9,36,37] The shift to a basal cell phenotype was confirmed by the loss of luminal keratins (*Krt7* and *Krt18*) and gain of basal keratins (*Krt1*, *Krt5*, *Krt6*, *Krt10*, *Krt13*, *Krt14*, *Krt15*, *Krt16*, *Krt17*, *Krt75*, and *Krt78*) in *Esr1*$^{-/-}$ EEO. A recent study in breast cancer epithelial cells found a strong negative correlation between basal keratin expression and *Esr1* levels,[51] in which the loss of ESR1-bound enhancers triggers upregulation of basal keratins.[52] Indeed, *Krt5*, *Krt6*, *Krt16*, and *Krt17* are overexpressed in *Esr1* mutant cells that undergo rapid clonal expansion and acquire stem-like properties in tumors.[53] Thus, ESR1 has a regulatory role in uterine epithelial lineage determination and homeostasis.

Cellular plasticity is a phenomenon in which cells change their identity or phenotype outside of conventional cell lineage determination pathways or tissue homeostasis and has been extensively documented in cancer.[34,54] Notably, cancer cells undergo changes in cell plasticity involving basal and luminal epithelial cells originating from shared bipotential progenitors, resulting in highly proliferative and invasive tumor phenotypes.[52,55] The multipotent epithelial cells lining the Müllerian duct and newborn female reproductive tract can differentiate into either uterine luminal-type or cervicovaginal basal-type epithelium.[1,2,4] The molecular mechanisms responsible for the loss of cellular identity through epithelial plasticity remain unclear;[34] however, recent studies have shown that the deletion of the tumor suppressor gene *Arid1a* induces basal differentiation and tumorigenesis in breast cancer cells by downregulating ESR1 target genes.[56,57] Similarly, disruptions in the interaction between high-order assemblies of transcription factors and ESR1-bound distal enhancers have been linked to the endocrine resistance-mediated upregulation of basal invasive markers in breast cancers following treatment with *Esr1* antagonists.[52] These findings underscore the intrinsic role of ESR1 in regulating luminal epithelial lineage determination and homeostasis in the uterus. However, additional studies will be required to fully understand the cell-intrinsic mechanisms of ESR1-mediated uterine epithelial differentiation.

In contrast to global *Esr1* null mice, epithelial-specific ablation of *Esr1* resulted in the appearance of basal cells and squamous metaplasia in the glands or necks of glands near the lumen of the adult uterus. However, basal cell differentiation was not detected in the epithelium of epithelial-specific *Esr1*-ablated mice on PND 30.[11,12] Thus, ESR1 has a biological role in the maintenance of the differentiated epithelial state in adult uteri. The emergence of basal cells in the uterine epithelium of the epithelial-specific *Esr1* cKO mice indicates that E2 acts via WT stroma to produce paracrine factors that alter differentiation of the ESR1-negative glandular epithelium and LE cells near the glands. Furthermore, these data suggest that the absence of stratification and basal epithelial signatures in the uterus of *Esr1*$^{-/-}$ and *Pgr*$^{Cre/+}$*Esr1*$^{f/f}$ females is the result of the lack of E2/ESR1 signaling in the stroma. The influence of the uterine mesenchyme/stroma on epithelial lineage determination and development has been long recognized. During neonatal development, the mesenchyme surrounding the Müllerian duct epithelium secretes paracrine factors (BMP4, ACTA, and FGF7/10) that activate p63 expression by mediating signaling pathways (SMAD4, RUNX1, and MAPK) in the epithelium.[5–8] Similarly, in the transition zone between the endo- and ectocervix of the adult mouse reproductive tract, the stroma drives the differential proliferation of specific epithelial cell lineages.[24] The stromal-epithelial organoid co-culture system employed here supports a requirement for factors produced by the endometrial stroma governing epithelial differentiation, homeostasis, and plasticity of *Esr1*$^{-/-}$ epithelial cells. Studies in breast cancer have provided evidence for a causal link between stromal signaling and the regulation of basal keratins (*Krt14*, *Krt16*, and *Krt17*) in *Esr1* mutant epithelium.[51] Here, E2 treatment of OVX mice resulted in the development of basal cells specifically in areas of *Esr1* deletion in the epithelium, whereas there was no evidence of basal cells in WT mice treated with E2. Similarly, treatment of co-cultures with E2 increased the expression of basal cell marker genes only in EEO lacking ESR1. These collective findings indicate that ESR1 has rather unexplored but important biological roles in mediating epithelial differentiation and cell lineage specification in response to paracrine factors produced by the stroma in response to E2.

In summary, our findings reveal that ESR1 regulates a gene regulatory network critical to maintain specified epithelial cell fate and plasticity in the uterus, as the absence of epithelial ESR1 leads to basal cell differentiation and squamous metaplasia in the adult uterus via paracrine signals produced by ESR1-positive stromal cells. Future studies should focus on unraveling the complex biology and nature of ESR1, E2, and stroma signals in the regulation of cellular plasticity and epithelial differentiation and homeostasis in the uterus. Those studies are important, because loss of ESR1 in the epithelium is linked to tumorigenesis, basal cell differentiation, and acquired endocrine resistance in several types of cancers.[58–61] Indeed, proper *Esr1* expression in the epithelium is likely critical to maintaining determined epithelial cell fate and homeostasis to prevent the development of endometrial hyperplasia and adenocarcinoma[34,52,58–61].

Limitations of the study

While these studies provide a thorough characterization of ESR1's role in uterine epithelial development, there are certain limitations to consider. *In vitro* studies utilizing EEO from global *Esr1*-null mice may not fully capture complex *in vivo* cell-cell interactions that take place in the tissue microenvironment of the developing uterus. Additionally, only WT stroma was evaluated for the co-culture system due to limitations in consistently obtaining confluent *Esr1*$^{-/-}$ stroma. Consequently, the study could not directly assess ESR1-independent E2 effects on stromal-epithelial interaction. Such interactions could provide additional information regarding the role of stromal-derived factors on basal cell differentiation in the absence of epithelial ESR1. Finally, the study did not use a human endometrial epithelial model to investigate whether the signaling identified in the mouse is conserved in humans.

STAR★METHODS

Detailed methods are provided in the online version of this paper and include the following:

- KEY RESOURCES TABLE

SUPPLEMENTAL INFORMATION

Supplemental information can be found online at https://doi.org/10.1016/j.isci.2023.107568.

ACKNOWLEDGMENTS

The authors would like to thank members of the Spencer and Kelleher laboratory for helpful discussions, the Jeong and Kim laboratory for support with histological analysis, and the University of Missouri Genomics Technology Core for assistance with library preparation and sequencing. This work was supported by the Eunice Kennedy Shriver National Institute of Child Health & Human Development of the National Institutes of Health Grants R01HD096266 (T.E.S.), R01HD097087 (W.W.), R01HD112315 (A.M.K), and new faculty start-up funds from the University of Missouri-Columbia (A.M.K.). The graphical abstract was created with BioRender.com.

AUTHOR CONTRIBUTIONS

J.A.R. and A.M.K. designed research; J.A.R., T.E.S., and A.M.K. performed research; W.W. provided critical reagents and mouse model for the study; J.A.R., K.M.D., T.E.S., and A.M.K. analyzed data; and J.A.R. and A.M.K. wrote the paper. All authors edited and approved the final manuscript.

DECLARATION OF INTERESTS

The authors declare no competing interests.

INCLUSION AND DIVERSITY

We support inclusive, diverse, and equitable conduct of research.

Received: June 15, 2023
Revised: July 11, 2023
Accepted: August 7, 2023
Published: August 9, 2023

REFERENCES

1. Orvis, G.D., and Behringer, R.R. (2007). Cellular mechanisms of Müllerian duct formation in the mouse. Dev. Biol. *306*, 493–504. https://doi.org/10.1016/j.ydbio.2007.03.027.
2. Mullen, R.D., and Behringer, R.R. (2014). Molecular genetics of Müllerian duct formation, regression and differentiation. Sex. Dev. *8*, 281–296. https://doi.org/10.1159/000364935.
3. Kelleher, A.M., DeMayo, F.J., and Spencer, T.E. (2019). Uterine glands: developmental biology and functional roles in pregnancy. Endocr. Rev. *40*, 1424–1445. https://doi.org/10.1210/er.2018-00281.
4. Cunha, G.R. (1976). Stromal induction and specification of morphogenesis and cytodifferentiation of the epithelia of the Müllerian ducts and urogenital sinus during development of the uterus and vagina in mice. J. Exp. Zool. *196*, 361–370. https://doi.org/10.1002/jez.1401960310.
5. Kurita, T., Cooke, P.S., and Cunha, G.R. (2001). Epithelial-stromal tissue interaction in paramesonephric (Müllerian) epithelial differentiation. Dev. Biol. *240*, 194–211. https://doi.org/10.1006/dbio.2001.0458.
6. Terakawa, J., Rocchi, A., Serna, V.A., Bottinger, E.P., Graff, J.M., and Kurita, T. (2016). FGFR2IIIb-MAPK Activity is required

for epithelial cell fate decision in the lower Müllerian duct. Mol. Endocrinol. *30*, 783–795. https://doi.org/10.1210/me.2016-1027.

7. Laronda, M.M., Unno, K., Ishi, K., Serna, V.A., Butler, L.M., Mills, A.A., Orvis, G.D., Behringer, R.R., Deng, C., Sinha, S., and Kurita, T. (2013). Diethylstilbestrol induces vaginal adenosis by disrupting SMAD/RUNX1-mediated cell fate decision in the Müllerian duct epithelium. Dev. Biol. *381*, 5–16. https://doi.org/10.1016/j.ydbio.2013.06.024.
8. Terakawa, J., Serna, V.A., Nair, D.M., Sato, S., Kawakami, K., Radovick, S., Maire, P., and Kurita, T. (2020). SIX1 cooperates with RUNX1 and SMAD4 in cell fate commitment of Mullerian duct epithelium. Cell Death Differ. *27*, 3307–3320. https://doi.org/10.1038/s41418-020-0579-z.
9. Kurita, T., Cunha, G.R., Robboy, S.J., Mills, A.A., and Medina, R.T. (2005). Differential expression of p63 isoforms in female reproductive organs. Mech. Dev. *122*, 1043–1055. https://doi.org/10.1016/j.mod.2005.04.008.
10. Kurita, T., Mills, A.A., and Cunha, G.R. (2004). Roles of p63 in the diethylstilbestrol-induced cervicovaginal adenosis. Development *131*, 1639–1649. https://doi.org/10.1242/dev.01038.
11. Nanjappa, M.K., Medrano, T.I., March, A.G., and Cooke, P.S. (2015). Neonatal uterine and vaginal cell proliferation and adenogenesis are independent of estrogen receptor 1 (ESR1) in the mouse. Biol. Reprod. *92*, 78. https://doi.org/10.1095/biolreprod.114.125724.
12. Lubahn, D.B., Moyer, J.S., Golding, T.S., Couse, J.F., Korach, K.S., and Smithies, O. (1993). Alteration of reproductive function but not prenatal sexual development after insertional disruption of the mouse estrogen receptor gene. Proc. Natl. Acad. Sci. USA *90*, 11162–11166. https://doi.org/10.1073/pnas.90.23.11162.
13. Cooke, P.S., Buchanan, D.L., Young, P., Setiawan, T., Brody, J., Korach, K.S., Taylor, J., Lubahn, D.B., and Cunha, G.R. (1997). Stromal estrogen receptors mediate mitogenic effects of estradiol on uterine epithelium. Proc. Natl. Acad. Sci. USA *94*, 6535–6540. https://doi.org/10.1073/pnas.94.12.6535.
14. Winuthayanon, W., Hewitt, S.C., Orvis, G.D., Behringer, R.R., and Korach, K.S. (2010). Uterine epithelial estrogen receptor α is dispensable for proliferation but essential for complete biological and biochemical responses. Proc. Natl. Acad. Sci. USA *107*, 19272–19277. https://doi.org/10.1073/pnas.1013226107.
15. Winuthayanon, W., Lierz, S.L., Delarosa, K.C., Sampels, S.R., Donoghue, L.J., Hewitt, S.C., and Korach, K.S. (2017). Juxtacrine activity of estrogen receptor α in uterine stromal cells is necessary for estrogen-induced epithelial cell proliferation. Sci. Rep. *7*, 8377. https://doi.org/10.1038/s41598-017-07728-1.
16. Couse, J.F., and Korach, K.S. (1999). Estrogen receptor null mice: what have we learned and where will they lead us? Endocr. Rev. *20*, 358–417. https://doi.org/10.1210/edrv.20.3.0370.
17. Miyagawa, S., and Iguchi, T. (2015). Epithelial estrogen receptor 1 intrinsically mediates squamous differentiation in the mouse vagina. Proc. Natl. Acad. Sci. USA *112*, 12986–12991. https://doi.org/10.1073/pnas.1513550112.
18. Huch, M., and Koo, B.K. (2015). Modeling mouse and human development using organoid cultures. Development *142*, 3113–3125. https://doi.org/10.1242/dev.118570.
19. Kim, J., Koo, B.K., and Knoblich, J.A. (2020). Human organoids: model systems for human biology and medicine. Nat. Rev. Mol. Cell Biol. *21*, 571–584. https://doi.org/10.1038/s41580-020-0259-3.
20. Xie, Y., Park, E.S., Xiang, D., and Li, Z. (2018). Long-term organoid culture reveals enrichment of organoid-forming epithelial cells in the fimbrial portion of mouse fallopian tube. Stem Cell Res. *32*, 51–60. https://doi.org/10.1016/j.scr.2018.08.021.
21. Ford, M.J., Harwalkar, K., and Yamanaka, Y. (2022). Protocol to generate mouse oviduct epithelial organoids for viral transduction and whole-mount 3D imaging. STAR Protoc. *3*, 101164. https://doi.org/10.1016/j.xpro.2022.101164.
22. Boretto, M., Cox, B., Noben, M., Hendriks, N., Fassbender, A., Roose, H., Amant, F., Timmerman, D., Tomassetti, C., Vanhie, A., et al. (2017). Development of organoids from mouse and human endometrium showing endometrial epithelium physiology and long-term expandability. Development *144*, 1775–1786. https://doi.org/10.1242/dev.148478.
23. Boretto, M., Maenhoudt, N., Luo, X., Hennes, A., Boeckx, B., Bui, B., Heremans, R., Perneel, L., Kobayashi, H., Van Zundert, I., et al. (2019). Patient-derived organoids from endometrial disease capture clinical heterogeneity and are amenable to drug screening. Nat. Cell Biol. *21*, 1041–1051. https://doi.org/10.1038/s41556-019-0360-z.
24. Chumduri, C., Gurumurthy, R.K., Berger, H., Dietrich, O., Kumar, N., Koster, S., Brinkmann, V., Hoffmann, K., Drabkina, M., Arampatzi, P., et al. (2021). Opposing Wnt signals regulate cervical squamocolumnar homeostasis and emergence of metaplasia. Nat. Cell Biol. *23*, 184–197. https://doi.org/10.1038/s41556-020-00619-0.
25. Lõhmussaar, K., Oka, R., Espejo Valle-Inclan, J., Smits, M.H.H., Wardak, H., Korving, J., Begthel, H., Proost, N., van de Ven, M., Kranenburg, O.W., et al. (2021). Patient-derived organoids model cervical tissue dynamics and viral oncogenesis in cervical cancer. Cell Stem Cell *28*, 1380–1396.e6. https://doi.org/10.1016/j.stem.2021.03.012.
26. Ali, A., Syed, S.M., and Tanwar, P.S. (2020). Protocol for *in vitro* establishment and long-term culture of mouse vaginal organoids. STAR Protoc. *1*, 100088. https://doi.org/10.1016/j.xpro.2020.100088.
27. Ali, A., Syed, S.M., Jamaluddin, M.F.B., Colino-Sanguino, Y., Gallego-Ortega, D., and Tanwar, P.S. (2020). Cell lineage tracing identifies hormone-regulated and Wnt-responsive vaginal epithelial stem cells. Cell Rep. *30*, 1463–1477.e7. https://doi.org/10.1016/j.celrep.2020.01.003.
28. Nikolakopoulou, K., and Turco, M.Y. (2021). Investigation of infertility using endometrial organoids. Reproduction *161*, R113–R127. https://doi.org/10.1530/REP-20-0428.
29. Candi, E., Schmidt, R., and Melino, G. (2005). The cornified envelope: a model of cell death in the skin. Nat. Rev. Mol. Cell Biol. *6*, 328–340. https://doi.org/10.1038/nrm1619.
30. Backendorf, C., and Hohl, D. (1992). A common origin for cornified envelope proteins? Nat. Genet. *2*, 91. https://doi.org/10.1038/ng1092-91.
31. Holthaus, K.B., Lachner, J., Ebner, B., Tschachler, E., and Eckhart, L. (2021). Gene duplications and gene loss in the epidermal differentiation complex during the evolutionary land-to-water transition of cetaceans. Sci. Rep. *11*, 12334. https://doi.org/10.1038/s41598-021-91863-3.
32. Hohl, D., Ruf Olano, B., de Viragh, P.A., Huber, M., Detrisac, C.J., Schnyder, U.W., and Roop, D.R. (1993). Expression patterns of loricrin in various species and tissues. Differentiation *54*, 25–34. https://doi.org/10.1111/j.1432-0436.1993.tb00656.x.
33. Banks-Schlegel, S., and Green, H. (1981). Involucrin synthesis and tissue assembly by keratinocytes in natural and cultured human epithelia. J. Cell Biol. *90*, 732–737. https://doi.org/10.1083/jcb.90.3.732.
34. Huyghe, A., Furlan, G., Schroeder, J., Cascales, E., Trajkova, A., Ruel, M., Stüder, F., Larcombe, M., Yang Sun, Y.B., Mugnier, F., et al. (2022). Comparative roadmaps of reprogramming and oncogenic transformation identify Bcl11b and Atoh8 as broad regulators of cellular plasticity. Nat. Cell Biol. *24*, 1350–1363. https://doi.org/10.1038/s41556-022-00986-w.
35. Keenan, A.B., Torre, D., Lachmann, A., Leong, A.K., Wojciechowicz, M.L., Utti, V., Jagodnik, K.M., Kropiwnicki, E., Wang, Z., and Ma'ayan, A. (2019). ChEA3: transcription factor enrichment analysis by orthogonal omics integration. Nucleic Acids Res. *47*, W212–W224. https://doi.org/10.1093/nar/gkz446.
36. Romano, R.A., Ortt, K., Birkaya, B., Smalley, K., and Sinha, S. (2009). An active role of the DeltaN isoform of p63 in regulating basal keratin genes K5 and K14 and directing epidermal cell fate. PLoS One *4*, e5623. https://doi.org/10.1371/journal.pone.0005623.
37. Schnittke, N., Herrick, D.B., Lin, B., Peterson, J., Coleman, J.H., Packard, A.I., Jang, W., and Schwob, J.E. (2015). Transcription factor p63 controls the reserve status but not the stemness of horizontal basal cells in the olfactory epithelium. Proc. Natl. Acad. Sci. USA *112*, E5068–E5077. https://doi.org/10.1073/pnas.1512272112.
38. Ho, M., Thompson, B., Fisk, J.N., Nebert, D.W., Bruford, E.A., Vasiliou, V., and Bunick, C.G. (2022). Update of the keratin gene family: evolution, tissue-specific expression patterns, and relevance to clinical disorders. Hum. Genom. *16*, 1. https://doi.org/10.1186/s40246-021-00374-9.
39. Wang, P., Wu, S.P., Brooks, K.E., Kelleher, A.M., Milano-Foster, J.J., DeMayo, F.J., and Spencer, T.E. (2018). Generation of mouse for conditional expression of Forkhead Box A2. Endocrinology *159*, 1897–1909. https://doi.org/10.1210/en.2018-00158.
40. Anderson, D.J., Marathe, J., and Pudney, J. (2014). The structure of the human vaginal stratum corneum and its role in immune defense. Am. J. Reprod. Immunol. *71*, 618–623. https://doi.org/10.1111/aji.12230.
41. Soyal, S.M., Mukherjee, A., Lee, K.Y.S., Li, J., Li, H., DeMayo, F.J., and Lydon, J.P. (2005). Cre-mediated recombination in cell lineages that express the progesterone receptor. Genesis *41*, 58–66. https://doi.org/10.1002/gene.20098.
42. Uetzmann, L., Burtscher, I., and Lickert, H. (2008). A mouse line expressing Foxa2-driven Cre recombinase in node, notochord, floorplate, and endoderm. Genesis *46*, 515–522. https://doi.org/10.1002/dvg.20410.
43. Jeong, J.W., Kwak, I., Lee, K.Y., Kim, T.H., Large, M.J., Stewart, C.L., Kaestner, K.H., Lydon, J.P., and DeMayo, F.J. (2010). Foxa2 is

essential for mouse endometrial gland development and fertility. Biol. Reprod. *83*, 396–403. https://doi.org/10.1095/biolreprod.109.083154.

44. Dhakal, P., Fitzgerald, H.C., Kelleher, A.M., Liu, H., and Spencer, T.E. (2021). Uterine glands impact embryo survival and stromal cell decidualization in mice. FASEB J *35*, e21938. https://doi.org/10.1096/fj.202101170RR.
45. Kelleher, A.M., Milano-Foster, J., Behura, S.K., and Spencer, T.E. (2018). Uterine glands coordinate on-time embryo implantation and impact endometrial decidualization for pregnancy success. Nat. Commun. *9*, 2435. https://doi.org/10.1038/s41467-018-04848-8.
46. Kelleher, A.M., Peng, W., Pru, J.K., Pru, C.A., DeMayo, F.J., and Spencer, T.E. (2017). Forkhead box a2 (FOXA2) is essential for uterine function and fertility. Proc. Natl. Acad. Sci. USA *114*, E1018–E1026. https://doi.org/10.1073/pnas.1618433114.
47. Kelleher, A.M., Burns, G.W., Behura, S., Wu, G., and Spencer, T.E. (2016). Uterine glands impact uterine receptivity, luminal fluid homeostasis and blastocyst implantation. Sci. Rep. *6*, 38078. https://doi.org/10.1038/srep38078.
48. Hancock, J.M., Li, Y., Martin, T.E., Andersen, C.L., and Ye, X. (2023). Upregulation of FOXA2 in uterine luminal epithelium and vaginal basal epithelium of epiERα-/-(*Esr1*$^{fl/fl}$*Wnt7a*$^{Cre/+}$) mice. Biol. Reprod. *108*, 359–362. https://doi.org/10.1093/biolre/ioac225.
49. Fitzgerald, H.C., Schust, D.J., and Spencer, T.E. (2021). In vitro models of the human endometrium: evolution and application for women's health. Biol. Reprod. *104*, 282–293. https://doi.org/10.1093/biolre/ioaa183.
50. Fitzgerald, H.C., Dhakal, P., Behura, S.K., Schust, D.J., and Spencer, T.E. (2019). Self-renewing endometrial epithelial organoids of the human uterus. Proc. Natl. Acad. Sci. USA *116*, 23132–23142. https://doi.org/10.1073/pnas.1915389116.
51. Li, Z., McGinn, O., Wu, Y., Bahreini, A., Priedigkeit, N.M., Ding, K., Onkar, S., Lampenfeld, C., Sartorius, C.A., Miller, L., et al. (2022). ESR1 mutant breast cancers show elevated basal cytokeratins and immune activation. Nat. Commun. *13*, 2011. https://doi.org/10.1038/s41467-022-29498-9.
52. Bi, M., Zhang, Z., Jiang, Y.Z., Xue, P., Wang, H., Lai, Z., Fu, X., De Angelis, C., Gong, Y., Gao, Z., et al. (2020). Enhancer reprogramming driven by high-order assemblies of transcription factors promotes phenotypic plasticity and breast cancer endocrine resistance. Nat. Cell Biol. *22*, 701–715. https://doi.org/10.1038/s41556-020-0514-z.
53. Gu, G., Tian, L., Herzog, S.K., Rechoum, Y., Gelsomino, L., Gao, M., Du, L., Kim, J.A., Dustin, D., Lo, H.C., et al. (2021). Hormonal modulation of ESR1 mutant metastasis. Oncogene *40*, 997–1011. https://doi.org/10.1038/s41388-020-01563-x.
54. Mills, J.C., Stanger, B.Z., and Sander, M. (2019). Nomenclature for cellular plasticity: are the terms as plastic as the cells themselves? EMBO J. *38*, e103148. https://doi.org/10.15252/embj.2019103148.
55. Rios, A.C., Fu, N.Y., Lindeman, G.J., and Visvader, J.E. (2014). In situ identification of bipotent stem cells in the mammary gland. Nature *506*, 322–327. https://doi.org/10.1038/nature12948.
56. Xu, G., Chhangawala, S., Cocco, E., Razavi, P., Cai, Y., Otto, J.E., Ferrando, L., Selenica, P., Ladewig, E., Chan, C., et al. (2020). ARID1A determines luminal identity and therapeutic response in estrogen-receptor-positive breast cancer. Nat. Genet. *52*, 198–207. https://doi.org/10.1038/s41588-019-0554-0.
57. Trizzino, M., Barbieri, E., Petracovici, A., Wu, S., Welsh, S.A., Owens, T.A., Licciulli, S., Zhang, R., and Gardini, A. (2018). The tumor suppressor ARID1A controls global transcription via pausing of RNA polymerase II. Cell Rep. *23*, 3933–3945. https://doi.org/10.1016/j.celrep.2018.05.097.
58. O'Brien, C.S., Howell, S.J., Farnie, G., and Clarke, R.B. (2009). Resistance to endocrine therapy: are breast cancer stem cells the culprits? J. Mammary Gland Biol. Neoplasia *14*, 45–54. https://doi.org/10.1007/s10911-009-9115-y.
59. Kabos, P., Haughian, J.M., Wang, X., Dye, W.W., Finlayson, C., Elias, A., Horwitz, K.B., and Sartorius, C.A. (2011). Cytokeratin 5 positive cells represent a steroid receptor negative and therapy resistant subpopulation in luminal breast cancers. Breast Cancer Res. Treat. *128*, 45–55. https://doi.org/10.1007/s10549-010-1078-6.
60. Brett, J.O., Spring, L.M., Bardia, A., and Wander, S.A. (2021). ESR1 mutation as an emerging clinical biomarker in metastatic hormone receptor-positive breast cancer. Breast Cancer Res. *23*, 85. https://doi.org/10.1186/s13058-021-01462-3.
61. Son, J., Park, Y., and Chung, S.H. (2018). Epithelial oestrogen receptor α is dispensable for the development of oestrogen-induced cervical neoplastic diseases. J. Pathol. *245*, 147–152. https://doi.org/10.1002/path.5069.
62. Schneider, C.A., Rasband, W.S., and Eliceiri, K.W. (2012). NIH Image to ImageJ: 25 years of image analysis. Nat. Methods *9*, 671–675. https://doi.org/10.1038/nmeth.2089.
63. Dobin, A., Davis, C.A., Schlesinger, F., Drenkow, J., Zaleski, C., Jha, S., Batut, P., Chaisson, M., and Gingeras, T.R. (2013). STAR: ultrafast universal RNA-seq aligner. Bioinformatics *29*, 15–21. https://doi.org/10.1093/bioinformatics/bts635.
64. Liao, Y., Smyth, G.K., and Shi, W. (2014). featureCounts: an efficient general purpose program for assigning sequence reads to genomic features. Bioinformatics *30*, 923–930. https://doi.org/10.1093/bioinformatics/btt656.
65. Robinson, M.D., McCarthy, D.J., and Smyth, G.K. (2010). edgeR: a Bioconductor package for differential expression analysis of digital gene expression data. Bioinformatics *26*, 139–140. https://doi.org/10.1093/bioinformatics/btp616.
66. Ge, S.X., Jung, D., and Yao, R. (2020). ShinyGO: a graphical gene-set enrichment tool for animals and plants. Bioinformatics *36*, 2628–2629. https://doi.org/10.1093/bioinformatics/btz931.
67. Hewitt, S.C., Kissling, G.E., Fieselman, K.E., Jayes, F.L., Gerrish, K.E., and Korach, K.S. (2010). Biological and biochemical consequences of global deletion of exon 3 from the ER alpha gene. FASEB J *24*, 4660–4667. https://doi.org/10.1096/fj.10-163428.
68. Jeong, J.W., Lee, H.S., Lee, K.Y., White, L.D., Broaddus, R.R., Zhang, Y.W., Vande Woude, G.F., Giudice, L.C., Young, S.L., Lessey, B.A., et al. (2009). Mig-6 modulates uterine steroid hormone responsiveness and exhibits altered expression in endometrial disease. Proc. Natl. Acad. Sci. USA *106*, 8677–8682. https://doi.org/10.1073/pnas.0903632106.

STAR★METHODS

KEY RESOURCES TABLE

REAGENT or RESOURCE	SOURCE	IDENTIFIER
Antibodies		
Mouse monoclonal anti-CDH1 (IF; 1:500)	BD Biosciences	Cat# 610182; RRID: AB_397581
Rabbit polyclonal anti-ESR1 (IF, WB; 1:2000, 1:1000)	Abcam	Cat# ab3575; RRID: AB_303921
Rabbit monoclonal anti-FOXA2 (IF, WB; 1:500, 1:1000)	Abcam	Cat# ab108422, RRID: AB_11157157
Rabbit polyclonal anti-KI67 (IF, 1:500)	Abcam	Cat# ab15580; RRID: AB_443209
Rabbit monoclonal anti-KRT5 (IF, 1:500)	Abcam	Cat# ab52635; RRID: AB_869890
Mouse monoclonal ani-KRT7 (IF, 1:500)	Santa Cruz	Cat# sc-23876; RRID: AB_2265604
Rabbit polyclonal anti-KRT14 (IF, 1:500)	LS Bio	Cat# ls-B3916; RRID: AB_10662336
Rabbit monoclonal anti-p63 (IF, 1:500)	Cell Signaling	Cat# 39692; RRID: AB_2799159
Rabbit polyclonal anti-p63 (WB, 1:1000)	Abcam	Cat# ab53039; RRID: AB_881860
Rabbit polyclonal anti-TUBA1B (WB, 1:10000)	Proteintech	Cat# 11224-1-AP; RRID: AB_2210206
Biotinylated goat anti-rabbit IgG (IHC, 1:1000)	Vector Laboratories	Cat# ba-1000; RRID: AB_2313606
Streptavidin-HRP (IHC, 1:1000)	Invitrogen	Cat# 434323; RRID: AB_2619743
HRP-conjugated goat anti-rabbit IgG (WB, 1:5000)	Fisher	Cat# 31460; RRID: AB_228341
Alexa Fluor 488, goat anti-rat IgG (IF 1:500)	Jackson ImmunoResearch	Cat# 112-545-143; RRID: AB_2338361
Alexa Fluor 647, goat anti-rabbit IgG (IF 1:500)	Jackson ImmunoResearch	Cat# 111-605-144; RRID: AB_2338078
Chemicals, peptides, and recombinant proteins		
Advanced DMEM/F12	Gibco	Cat# 12634010
B27 Supplement	Gibco	Cat# 12587010
Insulin-transferrin-selenium	Gibco	Cat# 41400045
Primocin	InvivoGen	Cat# Ant-pm
Glutamax	Gibco	Cat# 35050061
A83-01	Gibco	Cat# 21041025
Murine EGF	BioGems	Cat# 9094360
Murine FGF-10	Peprotech	Cat# AF-315-09
Murine R-spondin1	Peprotech	Cat# 450-61
Murine Noggin	Peprotech	Cat# 315-32
Murine Wnt3a	Peprotech	Cat# AF-250-38
Nicotinamide	Peprotech	Cat# AF-315-20
N2	BioGems	Cat# 9899208
DMEM/F12, no phenol red	Life Technologies	Cat# 17502048
Trypsin	Sigma	Cat# T4799
Hank's Balanced Salt Solution	Gibco	Cat# 14175
Soybean trypsin inhibitor	Gibco	Cat# 17075029
DNAse I	Roche	Cat# 10104159001
Cultrex BME	R&D Systems	Cat# 3445-005-01
Dimethyl sulfoxide	Fisher	Cat# D2650
Fetal bovine serum	Sigma	Cat# D1391
Collagenase V	Sigma	Cat# C9263
Easystrainer (70 µm)	Greiner Bio-One	Cat# 542070
Culture flask (25 cm^2)	Greiner Bio-One	Cat# 690195
DMEM/F12	Gibco	Cat# 11320033

(*Continued on next page*)

Continued

REAGENT or RESOURCE	SOURCE	IDENTIFIER
Antibiotic-Antimycotic (100X)	Gibco	Cat# 15240062
TrypLE, no phenol red	Gibco	Cat# 12563011
Flowmi cell strainers (40 μm)	Sigma	Cat# BAH136800040
Trypsin-EDTA (0.25%)	ThermoFisher	Cat# 25200056
Transwell inserts (0.4 μm PET membrane)	Corning	Cat# 353090
17β-estradiol	Sigma	Cat# E1024
Paraformaldehyde (96%)	Fisher	Cat# AC416780030
EM grade paraformaldehyde (16%)	Electron Microscopy Science	Cat# 15710
Agarose	Fisher	Cat# BP1356
Sodium citrate dihydrate	Fisher	Cat# BP327
Hydrogen Peroxide, 30%	Fisher	Cat# H325-500
Normal goat serum	Invitrogen	Cat# 01-6201
Permount	Fisher	Cat# SP15-500
Hematoxylin solution, Harris modified	Sigma	Cat# HHS32
Methanol	Fisher	Cat# A452-4
Phosphatase Inhibitor Cocktail 3	Sigma	Cat# P0044
Phosphatase Inhibitor Cocktail 2	Sigma	Cat# P5726
Protease Inhibitor Cocktail	Sigma	Cat# 11697498001
TRIzol Reagent	Invitrogen	Cat# 15596026
Critical commercial assays		
DAB ImmPACT substrate kit	Vector Laboratories	Cat# SK-4100
Hoechst 33342	Invitrogen	Cat# H3570
ProLong™ Diamond Antifade Mountant	Invitrogen	Cat# 36961
Bradford reagent	Bio-Rad	Cat# 50000006
Mini-PROTEAN TGX stain-free gels (4-20%)	Bio-Rad	Cat# 4568096
SuperSignal™ West Pico PLUS	Thermo Scientific	Cat# 34580
Direct-zol RNA Miniprep Plus Kits	Zymo Research	Cat# R2070
RNase-Free DNase I Set	Qiagen	Cat# 79254
iScript™ cDNA Synthesis Kit	Bio-Rad	Cat# 1708890
SsoAdvanced Universal SYBR Green Supermix	Bio-Rad	Cat# 1725274
Deposited data		
Transcriptome data from this study	Gene Expression Omnibus	GEO: GSE232655
Experimental models: Organisms/strains		
Mice: *Esr1*$^{-/-}$	Kindly provided by Dr. Dennis Lubahn (University of Missouri, Columbia, MO)	N/A
Mice: *Pgr*^{Cre}	Kindly provided by Dr. Francesco Demayo (NIEHS, Durham, NC) and Dr. John Lydon (Baylor College of Medicine, Houston, TX).	N/A
Mice: *Foxa2*^{Cre}	Kindly provided by Dr. Heiko Lickert (Helmholtz Zentrum München, Institute of Stem Cell Research, Neuherberg, Germany)	N/A
Mice: *Wnt7a*^{Cre}	The Jackson Laboratory	JAX stock #036637
Mice: *Esr1*$^{f/f}$	The Jackson Laboratory	JAX stock #032173

(*Continued on next page*)

Continued

REAGENT or RESOURCE	SOURCE	IDENTIFIER
Oligonucleotides		
Primers for Realtime PCR, see Table S4	This paper	N/A
Software and algorithms		
ImageJ	Schneider et al., 2012[62]	https://imagej.nih.gov/ij/
GraphPad Prism v 9.5.1	GraphPad Software	www.graphpad.com
FastQC v0.11.7.	The Babraham Institute	https://www.bioinformatics.babraham.ac.uk/projects/fastqc/
Trim Galore! V 0.6.6	The Babraham Institute	https://github.com/FelixKrueger/TrimGalore
STAR v 2.7.10b	Dobin et al., 2013[63]	https://github.com/alexdobin/STAR
featureCounts v 2.0.3	Liao et al., 2014[64]	https://subread.sourceforge.net/
edgeR *robust*	Robinson et al., 2010[65]	https://support.bioconductor.org/p/79149/
ShinyGO 0.77	Ge et al., 2020[66]	http://bioinformatics.sdstate.edu/go/
ChEA3	Keenan et al., 2019[35]	https://maayanlab.cloud/chea3/

RESOURCE AVAILABILITY

Lead contact

Further information and requests for resources and reagents should be directed to and will be fulfilled by the lead contact, Andrew M. Kelleher (andrew.kelleher@missouri.edu).

Materials availability

This study did not generate new unique reagents.

Data and code availability

- All data reported in this paper will be shared by the lead contact upon request. Raw FASQ data files are publicly available in the NCBI Gene Expression Omnibus (GSE232655).
- This paper does not report original code.
- Any additional information required to analyze the data reported in this paper is available from the lead contact upon request.

EXPERIMENTAL MODEL AND STUDY PARTICIPANT DETAILS

Mice

Floxed *Esr1* mice[67] were crossed with Pgr^{Cre},[41] $Foxa2^{Cre}$,[42] or $Wnt7a^{Cre}$[14] mice to generate conditional knockout animals. Pgr^{Cre} mice[41] were provided by Dr. Francesco Demayo (National Institute of Environmental Health Sciences, Durham, North Carolina) and Dr. John Lydon (Baylor College of Medicine, Houston, Texas). The $Foxa2^{Cre}$ mice[42] were provided by Dr. Heiko Lickert (Helmholtz Zentrum München, Institute of Stem Cell Research, Neuherberg, Germany). $Esr1^{-/-}$ mice[12] were provided by Dr. Dennis Lubahn (University of Missouri, Columbia, Missouri). $Wnt7a^{Cre}$[14] and Floxed *Esr1* ($Esr1^{f/f}$) mice were obtained from The Jackson Laboratory (Jax stock #036637 and #032173, respectively). Day of birth was considered postnatal day (PND) 0 in all studies. All animal procedures were approved by the Institutional Animal Care and Use Committee of the University of Missouri, Columbia and were conducted according to the NIH Guide for the Care and Use of Laboratory Animals.

Mouse endometrial epithelial organoids (EEO)

Uteri were removed from mice and digested in 1% trypsin (Sigma, T4799) in calcium and magnesium-free HBSS (Gibco, 14175-095) for 45 minutes at 4°C followed by 45 minutes at 37°C using an orbital shaker. The digestion was stopped with 1% soybean trypsin inhibitor (Gibco, 17075-029) in HBSS with 5 mM MgCl2 and 0.1 mg/mL DNAse-1 (Roche, 10104159001). For PND 15, Pasteur pipettes were carefully forged to create a slightly smaller diameter than the uterus, and sheets of epithelium retrieved by gentle suction using a mouth pipette. For PNDs 30 and 60, the digested uterine horns were gently squeezed with forceps. The epithelial tube sheets from each uterus were rinsed gently with HBSS and placed into 1.5 mL Eppendorf tubes. After centrifugation (300 x *g* for 3 minutes), the supernatant was removed, and epithelium pellet resuspended in base organoid media (Table S3). Following another round of centrifugation, the epithelium pellet was resuspended in 80% Cultrex (R&D Systems, 3445-005-01) and 20% organoid expansion media (Table S3). EEO were passaged (1:3 ratio) every 7-10 days. To

passage the EEO, Cultrex/EEO drops were detached from the cell culture plate by gentle pipetting and transferred into 1.5 mL Eppendorf tubes. After centrifugation (300 x *g* for 3 minutes), the supernatant was removed, replaced by 1.5 mL of HBSS, and pipetted up and down to dissociate the pellet. Following an additional centrifugation step, the cell pellet was resuspended in Cultrex and plated in 12-well plates (25 μL drops; 4 drops per well). Cultrex drops were incubated at 37°C for 15 min prior to adding 800 μL of organoid expansion media per well. Organoid cryopreservation was performed with freezing medium consisting of 10% DMSO in fetal bovine serum (FBS, Sigma, F0926) as described previously.[50] All experiments were performed using passage 3 EEO. Brightfield images were captured on a Leica DMi8 inverted microscope and Leica K8 camera using Leica Application Suite X (LAS X).

Isolation and culture of uterine stromal cells

Stromal cells were isolated from the uterus of adult WT females. First, the epithelium was removed from the uterus of 4-5 females as described previously. Uteri were then pooled, minced with scissors, transferred into a 15 mL Falcon tube, and digested in 10 mL of HBSS containing 0.1 mg/mL collagenase V (Sigma, C-9263) and 0.1 mg/mL DNAse-1 at 37°C for 30 minutes on an orbital shaker (80 RPM). The digested tissue was then filtered through a 70 mm nylon filter (Greiner Bio-One, 542070), and the filtrate containing stromal cells transferred to 25 cm^2 flasks (Greiner Bio-One, 690195). Stromal cells were cultured in DMEM/F12 (Gibco, 11320-033) with 10% FBS and 1% antibiotic-antimycotic (Anti-Anti, Gibco, 15240-062) at 37°C in a humidified 5% CO_2 environment. After 6 h, the media was changed to remove unattached and dead cells. After reaching 80% confluency, cells were utilized for co-culture experiments.

METHOD DETAILS

In vivo studies

For fertility studies, individual adult (6-8 weeks of age) *Esr1*$^{f/f}$ (WT) and *Foxa2*$^{Cre/+}$*Esr1*$^{f/f}$ females were placed with a CD-1 male mouse of proven fertility for six months, and the number of litters and pups born during that period were recorded.

For the E2 treatment study, WT and *Foxa2*$^{Cre/+}$*Esr1*$^{f/f}$ females were ovariectomized (OVX) at PND 30 and implanted with a sham implant as a control or a pellet containing 20 μg 17β-estradiol.[68] All mice were collected on PND 40 for analysis. Uterine gross morphology was recorded, and tissues were fixed in 4% paraformaldehyde for subsequent histological analysis.

Organoid formation assay

Passage 2 EEO embedded in Cultrex were transferred into a 5 mL Eppendorf tube. The EEO suspension was centrifuged (300 x *g* for 3 minutes at 4°C), the supernatant was removed, and the pellet was resuspended in 5 mL HBSS. Following an additional centrifugation step, the supernatant was removed, and the pellet was resuspended in 1 mL TrypLE (Gibco, 12563011) in a 1.5 mL Eppendorf tube. The cells were incubated in TrypLE for 10 minutes at 37°C on an orbital shaker. Following digestion, the cells were centrifuged at 300 x *g* for 3 minutes at 4°C, the supernatant was removed, and the pellet was resuspended in 500 mL base organoid media via gentle pipetting to create a single cell suspension. The cell resuspension was passed through a 40 mm cell strainer (Flowmi, Sigma, BAH-136800040), and filtered cells pelleted by centrifugation at 300 x *g* for 3 minutes at 4°C. Cell number and viability were assessed with a Countess™ II FL Automated Cell Counter (Invitrogen, AMQAX2000) prior to plating to ensure homogenous single-cell suspensions across samples (Figure S2). All organoid formation assays were conducted using at least three biological (mice) and three technical (wells) replicates (5000 cells/25 μL drops; 2 drops per well). Organoid formation efficiency and diameter were analyzed using ImageJ,[62] and the data are presented as the mean ± SEM. Statistical differences between two groups were determined with Student's t-test (GraphPad Prism 9), and statistical significance was defined as $p < 0.05$.

Co-culture of epithelial organoids and stroma

All co-culture experiments were performed using stromal cells from WT uteri, and EEO established from epithelium isolated from individual PND 30 uteri. For stroma seeding, stromal fibroblasts were detached from flasks using 0.25% trypsin (Gibco, 25200056), washed with HBSS, recovered by centrifugation, resuspended in 1.5 mL stromal cell medium (DMEM/F12 with 10% FBS and 1% Anti-Anti), and plated into 6-well plates (150K cells per well). For organoid establishment, uterine epithelial cells were isolated as described above. Briefly, after the second round of centrifugation, cell pellets were resuspended in 200 mL of 80% Cultrex: 20 % expansion media mix and divided into two 6-transwell inserts (0.4 μm pores, Corning, 353090), each containing 4 drops of 25 mL Cultrex mix. Inserts/Cultrex drops were then incubated at 37°C for 15 min. Next, the transwell inserts/Cultrex drops were placed into 6-well plates that either contained uterine stromal cells or did not contain any cells. For E2 treatment, vehicle (100% ethanol) or 100 nM E2 (17β-estradiol, Sigma, E1024; diluted in 100% ethanol) were added to phenol red-free organoid expansion media (Table S3) prior to culture. A total of 3 mL of media was added to the co-culture [1.5 mL per well (bottom) and 1.5 mL per insert (top)]. Fresh expansion media supplemented with vehicle or E2 was added to each well and insert every 72 h. New primary uterine stromal fibroblasts were isolated and seeded every 5 days, and EEO were passage into a new insert every 6-8 days. Co-cultures were documented every 5 days by brightfield microscopy. Following 20 days in culture, EEO were collected for RNA analysis. EEO derived from 3-7 females per genotype (WT or *Esr1*$^{-/-}$) were used for each co-culture experiment. Images were taken with a Leica DMi8 inverted microscope and Leica K8 camera using Leica Application Suite X (LAS X). EEO number and diameter were analyzed using ImageJ and the data are presented as the mean ± SEM. Statistical differences between two groups were determined with Student's t-test (GraphPad Prism 9) and statistical significance was defined as $p < 0.05$.

Organoid and tissue preparation

At least four Cultrex drops were examined per mouse, timepoint, and genotype. EEOs cultured in 12-well plates were washed with HBSS, fixed using warm 4% EM grade paraformaldehyde (Electron Microscopy Sciences, 15710) for 15 min at room temperature, stained with hematoxylin for 10 min, and washed with HBSS twice to remove excess staining. EEOs were then embedded using 1.5 mL of 2% agar (Fisher, BP1356) in HBSS per well and incubated overnight at 4°C with a wet pad to let blocks solidify. EEO blocks were carefully removed from the wells and placed in tissue cassettes. For tissue processing, uteri from 3-6 females were collected per time point, genotype, and treatment. Uteri were fixed in 4% paraformaldehyde in PBS overnight. EEO blocks and fixed uteri were dehydrated in ethanol, embedded in paraffin wax, and sectioned (7 μm).

Immunofluorescence and immunohistochemistry

Sections were mounted on slides, baked for 30 min at 60°C, deparaffinized in xylene, and rehydrated in a graded alcohol series. Deparaffinized sections were subjected to antigen retrieval by incubating sections in 10 mM citrate buffer (pH 6.0) at 95°C for 15 min, followed by cooling to room temperature. For peroxidase-based staining, sections were incubated with 5% H_2O_2 diluted in methanol for 12 minutes. All slides were blocked with 2% (v/v) normal goat serum (Invitrogen, 01-6201) in PBS at room temperature for 1 h and incubated with primary antibodies (see key resources table) overnight at 4°C in 1% BSA diluted in PBS. For peroxidase-based staining, the slides were washed in PBS and incubated with biotinylated secondary goat anti-rabbit antibody (1:1000 dilution; Vector Labs, Catalog # BA-1000) for 1 h at room temperature, followed by incubation for 45 min with Streptavidin HRP diluted in PBS (1:1000 dilution; Invitrogen, 434323). Signal was developed using Vector Labs DAB ImmPACT staining according to the manufacturer's instructions (Vector Labs, SK-4100). Sections were lightly counterstained with hematoxylin before affixing coverslips with Permount (Fisher, SP15-500). Immunofluorescence visualization was performed with Alexa 488 or Alexa 647-conjugated secondary antibodies (1:500 dilution; Jackson ImmunoResearch, #112-545-143, #111-605-144). Sections were counterstained with Hoechst 33342 (2 μg/mL; Invitrogen, H3570) before affixing coverslips with ProLong™ Diamond Antifade Mountant (Invitrogen, 36961). Images were taken with a Leica DM6 B upright microscope and Leica K8 camera using Leica Application Suite X (LAS X).

Western blot analysis of organoids

EEOs from 3 wells (12 Cultrex drops) were harvested and the Cultrex was removed. The resulting cell pellet was lysed in Cell Lysis Buffer (20 mM Tris-HCl pH 7.5, 150 mM NaCl, 1 mM EDTA, 1 mM EGTA, 1% NP-40, 1% sodium deoxycholate, 0.1% SDS) containing: 1x phosphatase inhibitor cocktail (Sigma-Aldrich, P0044, P5726) and 1x complete protease inhibitor cocktail (Roche, 11697498001). The lysates were incubated at 4°C for 30 minutes on an orbital shaker and clarified by centrifugation at 21,000 RCF in a microfuge for 15 minutes at 4°C. Protein concentrations in the lysates were determined using Bradford reagent (Bio-Rad, 50000006). The lysates were run on stain free 4-20% Mini-PROTEAN TGX Precast gels (Bio-Rad, 456-8096) and transferred to a nitrocellulose membrane. The membranes were blocked with 5% nonfat milk in TBST for 1 h at room temperature. After washing, the membranes were incubated with primary antibodies (see key resources table) in 1% nonfat milk made in TBST overnight at 4°C, followed by anti-rabbit HRP-conjugated IgG (1:5000; Thermo Fisher, 31460) for 1 h at room temperature. Western blot signals were detected using an ECL detection reagent (Thermo Fisher, 34580).

RNA isolation and real-time PCR (RT-qPCR)

Samples were collected at the indicated time points and total RNA was isolated using the Direct-zol kit (Zymo Research, R2070) according to the manufacturer's instructions. To eliminate genomic DNA contamination, RNA was treated with DNase I (Qiagen, 79254) during RNA isolation. The quantity and purity of total RNA were determined using a Nanodrop spectrophotometer (Fisher, 840274200). Total RNA was reverse transcribed to synthesize cDNAs for each sample using an iScript™ cDNA Synthesis Kit (Bio-Rad, 1708890). The cDNA samples were subjected to qPCR using gene-specific primers (Table S4). Briefly, real-time qPCR amplification of cDNAs was carried out in a reaction mixture (10 μL) containing SsoAdvanced Universal SYBR Green Supermix (Bio-Rad, 1725274) and primers (250 nM each). A CFX384 Touch Thermal Cycler (Bio- Rad, 1851138) was employed to perform PCR using a two-step protocol with initial denaturation/enzyme activation at 95°C for 30 s, followed by 40 cycles of denaturation at 95°C for 5 s, and annealing/extension for 30 s at 60°C. Samples were analyzed in duplicates and melting curve analyses were performed to ensure specific amplification of the targeted amplicon. Target gene expression was normalized to the expression of *Actb* and *Ppia* mRNA. Relative expression was determined in comparison to the value of an appropriate control sample. All experiments were performed at least three times with independent biological replicates. Statistical differences between two groups were determined using Student's t-test (GraphPad Prism 9) and statistical significance was defined as $p < 0.05$.

Library preparation and RNA-sequencing

Biological replicates were generated by pooling total RNA from 3 wells of EEOs per female (n=3 females/genotype/treatment). RNA was isolated using a Direct-zol kit (Zymo Research, R2070) according to the manufacturer's instructions. The quality and concentration of RNA were determined using a Fragment Analyzer (Agilent, Santa Clara, CA, USA). Libraries were prepared by the University of Missouri DNA core using an Illumina TruSeq mRNA kit (Illumina Inc., San Diego, CA, USA) and sequenced (paired end 150; 30 million read pairs) using an Illumina NovaSeq 6000.

Differential expression analysis

Quality of raw data before and after trimming was assessed using FastQC v0.11.7. Adapters and low-quality bases (Phred score < 20) were trimmed from reads using Trim Galore! V0.6.6. The reads were then mapped to the mouse reference genome (GRCm39) using STAR v2.7.10b[63] with transcript annotation index in R v4.2.2. Raw read counts per gene were quantified with featureCounts v2.0.3.[64] Differential expression analysis was conducted using edgeR *robust*, a method demonstrably robust in conducting exact tests of significance suitable for small counts and limited numbers of biological replicates.[65] Differentially expressed genes (DEG) between WT and KO were determined at Log2 fold change > 2, FDR < 0.05, and mean CPM > 1 and carried forward for further analyses. Heatmaps were visualized using the "pheatmap" package in R v4.2.2. Enriched gene ontology biological processes and network analysis were determined with ShinyGO.[66] Transcription factors with binding sites enriched in annotated promoter regions of DEG were determined with ChEA3 using a database of publicly available ChIP-seq experiments derived from literature.[35]

QUANTIFICATION AND STATISTICAL ANALYSIS

All western blots with quantification were performed with at least three independent biological replicates and analyzed using Image Lab Software (Bio-Rad). The data are presented as the mean ± SEM, as determined from at least three independent experiments. Following the Shapiro-WILK test for normality, the data were analyzed using Student's t-test (GraphPad Prism 9). A p-value of less than 0.05 was considered statistically significant. Statistical analyses for the genomic experiments were performed using standard genomic statistical tests as described above.